

## RESEARCH ARTICLE

## Killed *Bacillus subtilis* spores expressing streptavidin: a novel carrier of drugs to target cancer cells

Van Anh Thi Nguyen<sup>1</sup>, Hong Anh Huynh<sup>2</sup>, Tong Van Hoang<sup>3</sup>, Ngoc Thi Ninh<sup>1</sup>, An Thi Hong Pham<sup>1</sup>, Hoa Anh Nguyen<sup>1,4</sup>, Tuan-Nghia Phan<sup>1</sup>, and Simon M. Cutting<sup>2</sup>

<sup>1</sup>Key laboratory of Enzyme and Protein Technology, VNU University of Science, Hanoi, Vietnam, <sup>2</sup>School of Biological Sciences, Royal Holloway, University of London, Egham, UK, <sup>3</sup>Department of Microbiology, Vietnam Military Medical University, Hadong, Hanoi, Vietnam, and <sup>4</sup>ANABIO Research & Development JSC, Van Khe, Hadong, Hanoi, Vietnam

**Abstract**

Carriers of drugs in cancer therapy are required to reduce side-effects of the drugs to normal cells. Here we constructed killed recombinant *Bacillus subtilis* spores (SA1) that expressed streptavidin as a chimeric fusion to the spore coat protein CotB and used the spores as bioparticle carrier. When bound with biotinylated cetuximab these spores could specifically target to the epidermal growth factor receptor on HT 29 colon cancer cells, thereby delivered paclitaxel to the cells with 4-fold higher efficiency, as indicated by fluorescent intensity of paclitaxel Oregon Green 488 bound to HT29 cells. Based on real-time monitoring of cell index, the IC<sub>50</sub> of growth of HT29 cells by paclitaxel-SA1-cetuximab was estimated to be 2.9 nM approximately 5-fold lower than water-soluble paclitaxel (14.5 nM). Instability of DNA content was observed when cells were treated with 16 nM paclitaxel-SA1-cetuximab, resulting in a 2-fold enhancement in polyploidy cells. Thus, by targeting the release of paclitaxel to HT29 cells, spore-associated cetuximab augmented the inhibitory effect of paclitaxel on cell division and proliferation. The SA1 could be used as a "universal" drug carrier to target specific biomarkers on cancer cells by conjugating with suitable biotinylated antibodies.

**Introduction**

The side-effects of the chemicals used in the treatment of cancer are potentially serious to cancer patients undergoing high-dose transfusions during long-term chemotherapy, mostly because of diffusion into whole body fluids, targeting and killing normal cells and damaging vital organs. To avoid this, chemotherapy should deliver and ensure localization of drugs to the immediate vicinity of the cancerous cells or tumors. Research on metallic and polymeric nanoparticles as drug carriers in medicine has grown rapidly due to the unique surface properties of nanoparticles that can be functionalized both for loading chemicals and conjugating biomolecules that can specifically target cancer cells. Most studies to date have been made with nanogolds and magnetic nanoparticles for specific delivery of chemicals to target cancer cells or tumors [1–3]. However, a number of limitations exist including the stability and uniformity of the functionalized particles as well as the potential health issues arising from the use of metallic or polymer nanoparticles [4]. Therefore, natural organic

bioparticles would be an ideal alternative carrier system with potential advantages in stability, uniformity and patient-friendly attributes. In recent years, Melezki and his colleagues have performed injecting spores of *Clostridium novyi-NT*, a genetic engineered clone of *C. novyi* in which a toxic virulent gene has been knocked out, into mice having cancer tumor, and they have found high binding ability of spores on cancer tumors. Therefore, population of spores surrounding the tumor can inhibit the growth of the tumor [5]. Other groups have developed recombinant *C. sporogenes* that highly express nitroreductase (NTR). The anaerobic spores will specifically accumulate at the tumors, thereby germinating and secreting NTR to convert prodrugs, namely CB1954 or 5-FC, to active drugs to kill the tumors. The trials in animal have shown that the growth of HTC116 tumors in mice has been substantially suppressed [6,7].

*Bacillus subtilis* is a Gram-positive bacterium that is able to produce heat-stable spores of about 1 µm diameter. This organism is genetically well studied and, in the spore form, is used worldwide as a probiotic supplement in humans [8]. The *B. subtilis* spore surface has a negative surface charge and is hydrophobic [9] with surface layers composed mostly of about 30 different protein species [10]. Based on their charge and hydrophobic properties *B. subtilis* has been shown to efficiently adsorb and bind protein antigens, for example, alpha toxin of *Clostridium perfringens* and tetanus toxin of *C. tetani* [9]. Virus particles have also been shown to adsorb

Address for correspondence: Van Anh Thi Nguyen, Key laboratory of Enzyme and Protein Technology, VNU University of Science, 334 Nguyen Trai, Hanoi, Vietnam, Tel: 84-(0)4-35579354. Fax: 84-(0)4-35575498. E-mail: vananhbiolab@gmail.com  
Simon M. Cutting, School of Biological Sciences, Royal Holloway, University of London, Egham, Surrey TW20 0EX, UK. Tel: 44-(0)1784-443760. Fax: +44-(0)1784-414224. E-mail: s.cutting@rhul.ac.uk

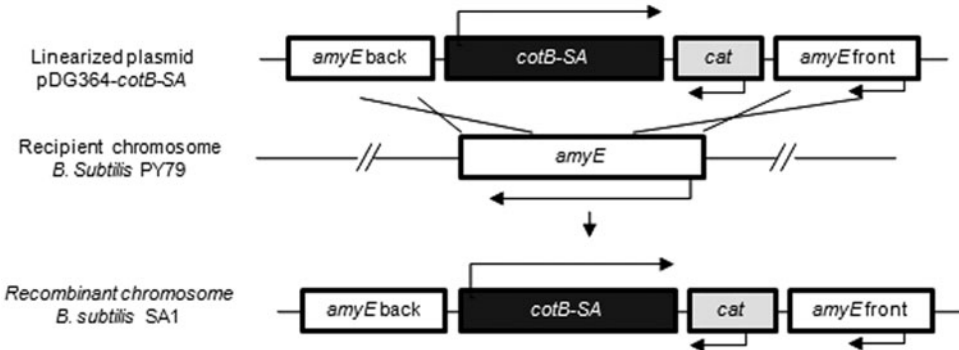


Figure 1. Strategy for the chromosomal integration of the *CotB-SA* gene. Arrows indicate direction of transcription.

to spores, for example, intact H5N1 virions adsorbed to killed *B. subtilis* spores which were used to nasally vaccinate mice and confer full protection to challenge with an H5N1 virus [11].

Extensive studies have been made describing genetic engineering to create heat-stable vaccine spores [12]. To date, antigens are most commonly expressed as fusion proteins with two spore-coat proteins, CotB and CotC [6,13–16]. Streptavidin (SA) has been successfully expressed as a fusion protein with the outer coat protein CotG on the outer surface of *B. subtilis* DB104 spores, as indicated by FACS and immunological methods. These streptavidin spores were shown to bind specifically to biotin-labeled fluorescent FITC, and have been expected to be a live diagnostic tool in biotechnology [17]. Since SA is a molecule of interest in molecular biology due to its extremely high affinity to biotin and biotinylated molecules [18–20], we engineered *B. subtilis* to express SA as a fusion to the outer spore coat protein CotB. These spores were bound specifically with biotinylated cetuximab, a chimeric IgG1 monoclonal antibody that targets the extracellular domain of epidermal growth factor receptor (EGFR) over-expressed on the surface of 30–85% colon cancer cell types, including cetuximab-sensitive HT29 cell lines [19–25]. The created biocomplexes “spores-cetuximab” through SA–biotin interaction demonstrated as efficient carriers for paclitaxel, a common chemical used in cancer therapy [26], and we examined their ability to target the colon cancer cells *in vitro*.

## Materials and methods

### Bacterial strains

*Bacillus subtilis* wild-type strain PY79 (*spo<sup>+</sup>*) was used. All recombinant strains described here are isogenic derivatives of PY79. Plasmid amplification for nucleotide sequencing, sub-cloning experiments and  $\text{CaCl}_2$ -mediated transformation of *E. coli* competent cells were performed in the *E. coli* strain DH5 $\alpha$ , as described in Sambrook et al. [27]. Methods for *Bacillus* including the two-step transformation of *B. subtilis* were those outlined in Cutting et al. [28].

### Construction of gene fusions

A segment of CotB carrying the complete promoter sequence and 825 5'-codons of its open reading frames (ORFs) were cloned in pDG364. pDG364 is a plasmid that enables ectopic insertion of heterologous DNA into the *B. subtilis* genome

[28] and the procedures were similar to the use of CotB for expression of antigens on the spore surface described previously [29]. The CotB promoter was polymerase chain reaction (PCR) amplified from the *B. subtilis* strain PY79 chromosome using oligonucleotide primers (forward, 5'-cgccggatccACGGATTAGGCCGTTGTCCT-3' having a restriction site for *Bam*H I and reverse 5'-cccaagcttGGATGA TTGATCATCT-3' having a restriction site for *Hind*III). The purified PCR product was cloned into pDG364 that had been digested with *Bam*H I and *Hind*III to generate pDG364-CotB.

Using *Streptomyces avidinii* strain 11996 (NCIMB Ltd., Aberdeen, UK) as a chromosomal template, the complete SA ORF was amplified using two primers (forward, 5'-aaaaagcttGACCCCTCCAAGGACTCGAAG-3' having a restriction site for *Hind*III and reverse 5'-aaagaattcCTACTG CTGAACGGCGTCGAG-3' having a restriction site *Eco*RI). Purified PCR-amplified SA DNA having the expected size of 500 bp was cleaved with *Hind*III and *Eco*RI and cloned into pDG364-CotB cleaved with *Hind*III and *Eco*RI. This created an in-frame fusion of CotB with SA at the *Hind*III site. The clone was verified using DNA sequencing across the fusion site and the plasmid linearized by digestion with *Pst*I. Linearized DNA was then used to transform competent cells of *B. subtilis* strain PY79 with selection of chloramphenicol-resistant colonies. Transformants carried a stable, double crossover, insertion of the *CotB-SA* chimera at the amylase gene (*amyE*) and the resulting clone is named SA1 (Figure 1).

### Preparation of spores and extraction of spore coat proteins

Sporulation of *B. subtilis* PY79 (*spo<sup>+</sup>*) and the *B. subtilis* strain (SA1) expressing CotB-SA was made in Difco sporulation media at 37°C using the exhaustion method. Sporulating cultures were harvested 60 h after the initiation of sporulation and suspensions of spores purified using lysozyme treatment to break any residual sporangial cells followed by washing in 1 M NaCl, 1 M KCl and water [30]. The number of spores was calculated by serial dilution and plate counting. Spores were killed by autoclaving (120°C, 15 p.s.i, 20 min). Water lost by evaporation was calculated and sterile water was added to restore to the original volume before autoclaving using microscopic counting of spore particles using a hemocytometer to determine spore counts. Hundred percent spore killing was validated by serial dilution and plate counting.

## Western analysis

Spore coat proteins were extracted from suspensions ( $1 \times 10^9$ ) of pelleted spores of PY79 and SA1 using 40 µl of an SDS-DTT extraction buffer [30]. Protein concentration was determined using the Bradford assay and approximately 20 µg was fractionated on 12% SDS-PAGE gels. Western blotting was used to detect the 50 kDa CotB-SA chimera (35 kDa of truncated CotB fused to 15 kDa of SA) using a polyclonal streptavidin-specific rabbit antibody (Sigma-Aldrich, St Louis, MO) and anti-rabbit IgG conjugated with horseradish peroxidase (Promega, Fitchburg, WI). Western blot membranes were visualized using the ECL (GE Healthcare Life Science, Sweden) method using ECL Plus™ Western Blotting Detection Reagents, following the manufacturer's instruction.

## Biotinylation and fluorescent labeling of cetuximab

Cetuximab was labeled with biotin and fluorescent Alexa 546 using methods described previously [11,31,32]. Cetuximab (Erbitux®, MerkSorono, Switzerland) at a concentration of 5 mg/ml was dialyzed overnight in phosphate saline buffer (PBS; 145 mM, pH 7.4) with two changes of buffer. The dialyzed cetuximab was centrifuged to remove precipitates and the concentration was adjusted to 2.4 mg/ml, equivalent to 20 µM. Next, it was used either for labeling with 40 µM succinimidyl biotin (Sigma-Aldrich, MO) or for dual labeling with a mixture of 40 µM succinimidyl biotin and 40 µM succinimidyl Alexa 546 (Life Technologies, NY, excitation/emission: 546 nm/580 nm) at room temperature (RT) for 1 h in PBS (pH 7.4; NaCl 137 mM). Reactions were stopped by adding 1 mM Tris-HCl, and the unreacted succinimidyl biotin and Alexa 546 dyes were carefully removed by sequential dialysis (three times) using a mini-dialysis kit with a 8 kDa cut-off (GE Healthcare Life Science, Sweden) in PBS. Biotinylated cetuximab and dual-labeled biotinylated-Alexa546 cetuximab were then centrifuged (100 000 rpm; 5 min) to remove precipitation that may have occurred during labeling and dialysis. The concentration of protein in the labeled sample was determined (using a NanoDrop® spectrophotometer ND-1000) to be 1 mg ml<sup>-1</sup>, equivalent to 8.3 µM of protein and 8.5 µM of Alexa-546, indicating a protein to dye ratio of about 1:1.

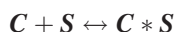
## Cetuximab binding

To measure binding constants, different amounts of biotinylated cetuximab ranging from 0.25 µg, 1 µg, 4 µg to 8 µg were bound on  $1 \times 10^9$  SA1 spores in PBS (pH 7.4; NaCl, 137 mM). In another experiment for pH-dependent binding determination, binding of 1 µg biotinylated cetuximab to  $1 \times 10^9$  SA1 spores was performed at different pH's ranging from 2 to 10 which was created by using suitable buffers containing 137 mM NaCl. Incubations were made in 300 µl buffers for less than 1 h and the unbound biotinylated cetuximab was removed using three washes with PBS (0.01 M, pH 7.4) before SDS-PAGE analysis. Biotinylated cetuximab bound with  $2 \times 10^8$  spores (one-fifth of the initial amount of spores incubated) was checked for the presence of a 60 kDa species indicating that DTT-reduced IgG by Western blotting using anti-human IgG-conjugated alkaline phosphatase (Promega, WI), and the purple color reaction determined using the NBT/BCIP

substrate (BioBasic, Canada). About 100 ng of biotinylated cetuximab was used as a positive control. The intensity of 60 kDa bands was analyzed using Scion Image® software.

## Binding constant and number of SA molecules expressed on SA1 spores

The binding constant  $K_{b(C-S)}$  of biotinylated cetuximab to CotB-SA on the spore surface and the number of binding sites SA ( $R_s$ ) per µm<sup>2</sup> of a spore for interaction with biotinylated cetuximab was determined as follows. The initial biotinylated cetuximab concentration was assigned as  $[C_o]$  in nM unit and the concentration of  $1 \times 10^9$  spores/300 µl was calculated as  $\sim 5.3 \times 10^{-3}$  nM and assigned as  $[S_o]$ , considering a single spore as one molecule. The concentration of biotinylated cetuximab bound to the membranes,  $[C_b]$ , was estimated by determining the intensity of the band in comparison to the intensity of the control using the Scion Image® software (NIH, NY). The data of  $[C_b]$  and  $[C_o]$  were included in the following equation for calculation of constant  $K_{b(C-S)}$  and  $R_s$  [31].



$$K_{b(C-S)} = \frac{[C * S]}{[C][S]} = \frac{[C_b]}{[C_o - C_b][R_s * S - C_b]}$$

## Immunofluorescence and direct fluorescence imaging

About  $1 \times 10^9$  and  $1 \times 10^9$  PY79 spores were fixed with ice-cold paraformaldehyde 1% for 15 min, then washed three times with PBS (145 mM, pH 7.4). Next, the spores were incubated with polyclonal SA-specific antibody at 10 mM for 45 min at RT, followed by anti-rabbit IgG-conjugated Alexa 546 at 10 mM for 45 min at RT. Incubations with antibodies were performed in the presence of 2% BSA and three washes with PBS (pH 7.4; NaCl 137 mM) plus 0.5% BSA after the first antibody. The spores were imaged under an excitation of 525 nm (green laser) using a confocal fluorescence microscope Carl Zeiss LSM510 (Carl Zeiss, Germany).

About  $1 \times 10^9$  SA1 spores and  $1 \times 10^9$  PY79 spores were treated in acetate buffer 30 mM pH 4.0 for 30 min, washed and suspended in PBS (145 mM pH 7.4). Next, 1 ml containing  $1 \times 10^8$  spores was incubated with both 200 nM paclitaxel Oregon Green 488 and 20 nM dual-labeled biotinylated-Alexa 546 cetuximab for 30 min. Spores were washed three times with PBS (145 mM, pH 7.4) to remove unbound chemicals and proteins and then observed under an excitation of 488 nm (blue laser) and 525 nm (green laser) for Oregon Green 488 and Alexa 546, respectively, using confocal fluorescence microscopy.

A colon cancer cell line HT29 (American Type Culture Collection, ATCC, NY) that over-expresses EGFR and that is cetuximab-sensitive [25,33] was cultured in cell culture flasks containing Roswell Park Memorial Institute-1640 medium (RPMI, Life Technologies, NY) supplemented with 10% heated fetal bovine serum (FBS, Sigma-Aldrich, MO). A human breast cancer cell line KPL-4 expressing high level of Her2/neub, but not EGFR which is sensitive to trastuzumab and resistant to cetuximab [34–36] (kindly provided by Prof. H. Higuchi, Biomedical Engineering Research Organization, Tohoku University, Japan) was cultured in cell culture flasks

containing Dulbecco's Modified Eagle Medium (DMEM, Life Technologies, NY) low glucose supplemented with 5% FBS. HT 29 that had been checked to be much more sensitive to cetuximab was compared to KPL4 by the immunofluorescent method using cetuximab labeled with Alexa 546. HT29 or KPL4 cells were further cultured individually in 24-well ELISA plates containing coverslips at the bottom of each well, either in RPMI-1640 or DMEM, respectively. The two cell lines were then used as targets to test the delivery of paclitaxel Oregon Green 488 (Life Technologies, NY; excitation/emission: 488 nm/525 nm) at a concentration of 1  $\mu$ M by cetuximab bound to SA1 spores. Negative controls (absence of paclitaxel) and other positive controls of water-soluble paclitaxel Oregon Green 488 and paclitaxel Oregon Green 488 adsorbed on the wild-type PY79 (paclitaxel-PY79) at the same 1  $\mu$ M concentration were performed in parallel. Incubation of cells and paclitaxel in different formulations was conducted within 6 h and the cells were washed (PBS, pH 7.4) three times to remove unbound paclitaxel and spores. The HT29 and KPL4 cells were then fixed using ice-cold paraformaldehyde (3.7% v/v) and triton X-100 (1% v/v) for 15 min at RT, followed by three times washing with PBS (pH 7.4; 137 mM NaCl) and DNA-staining using the diamidino-2-phenylindole (DAPI) fluorescent dye (Life Technologies, NY; excitation/emission: 358 nm/461 nm) at 0.1 mg/ml for 20 min. After this, coverslips containing either HT29 or KPL4 cells were washed to remove remaining DAPI and finally sealed using the aqueous mounting medium Permaflour® (Beckman Coulter, Germany) for observation. The cells were observed under an excitation of 320 nm (using UV light of mercury lamp and of 480 nm (blue laser) using a confocal fluorescence microscope. The off-set was made in the case of KPL4 cells to remove the background of the green signal due to autofluorescence. The intensity of paclitaxel bound in the cells was analyzed using Scion Image® software (NIH, NY).

### Fluorospectrometer analysis of binding of paclitaxel and its dissociation rate

PY79 spores and biotinylated cetuximab bound SA1 spores were treated in acetate buffer 30 mM pH 4.0 for 30 min, washed (in PBS) and suspended in PBS buffer (145 mM pH 7.4). Next, 1 ml of PY79 or SA1 spores ( $1 \times 10^8$ ) were incubated with paclitaxel Oregon Green 488 at concentrations ranging from 200 nM to 1  $\mu$ M at 25 °C for 1 h. Unbound paclitaxel Oregon Green 488 ( $P_s$ ) was obtained by centrifuging the spores at 12 000 rpm for 3 min, and measured using a fluorospectrometer under an excitation of 480 nm. The initial concentrations of paclitaxel ( $P_o$ ) applied to spores were determined by performing parallel incubations in the absence of the spores. Experiments were performed in triplicate and the detectable resolution was 100 pM fluorophores.

### Dissociation rates of biotinylated cetuximab and paclitaxel from spores

Dissociation rate constants of biotinylated cetuximab from SA1 spores  $k_{off(C-S)}$  were determined by incubating  $1 \times 10^9$  saturated cetuximab-bound SA1 spores in 1 ml PBS at different time points (0 h, 1 h, 2 h, 4 h, 8 h, 24 h, 48 h, 72 h, 7 d, 14 d). Dissociation rate constants of paclitaxel Oregon

Green 488 from SA1-cetuximab  $k_{off(P-SA1-cetuximab)}$  were determined by incubating  $1 \times 10^8$  paclitaxel-Oregon bound SA1-cetuximab spores either in 1 ml PBS in different pH buffers ranging from 2 to 8 at different time points (0 h, 1 h, 2 h, 4 h, 8 h, 24 h, 48 h, 72 h, 7 d, 14 d), or in 1 ml of human serum (donated by a healthy volunteer) at different time points (0 h, 2 h, 4 h, 8 h, 24 h, 48 h). In the case of paclitaxel Oregon Green 488 (10X greater than non-labeled paclitaxel) was added to either PBS buffer or the human serum at a final concentration of 10  $\mu$ M. Next, the amount of cetuximab bound on SA1-spores and paclitaxel bound on SA1-cetuximab spores were measured again using Western blotting and fluorospectrometry, respectively. The dissociation rate constants  $k_{off(C-S)}$  and  $k_{off(P-SA1-cetuximab)}$  were calculated based on the following equations:  $k_{off} = 0.693/t_{1/2} \text{ min}^{-1}$  while  $t_{1/2}$  is the half-life when binding falls below 50%.

### Real-time electrical recording of cell proliferation

Cells were cultured in an E-plate96 and placed on an RTCA SP station connected to an RTCA analyzer (Roche Applied Science, Switzerland) for real-time electrical recording of cell proliferation. In detail, HT29 was cultured in 200  $\mu$ l of RPMI and 200  $\mu$ l KPL4 was cultured in DMEM at an initial concentration of 10 000 cells/well and 2000 cells/well, respectively. For preparation of PY79-cetuximab and SA1-cetuximab, 1  $\mu$ g cetuximab biotinyl was adsorbed with either  $10^9$  PY79 or  $10^9$  SA1, and the unbound cetuximab was washed off from the spores. In an experiment to test toxicity of SA1-cetuximab,  $1 \times 10^8$  SA1,  $1 \times 10^8$  SA1-cetuximab spores and 20 ng cetuximab were added into each well containing 200  $\mu$ l medium at the beginning of cell incubation and observation. In later experiments to test activity of paclitaxel bound SA1-cetuximab, cells were grown and attached to the sensors for 24 h before adding paclitaxel either in water-soluble form, paclitaxel-PY79 or paclitaxel-SA1-cetuximab. The concentration of PY79 and SA1-cetuximab was  $1 \times 10^6$  cfu/200  $\mu$ l medium and the concentration of paclitaxel ranged from 1 nM to 1  $\mu$ M. As controls, a negative control was 200  $\mu$ l of DMEM and RPMI only and negative controls in each well for substrates included  $1 \times 10^6$  PY79, cetuximab (20 ng),  $1 \times 10^6$  PY79-cetuximab, and  $1 \times 10^6$  SA1-cetuximab in RPMI medium. Wells of each sample were repeated three times. Further incubation after addition of paclitaxel was conducted for an additional two days for KPL4 and three days for HT29. The process of cell growth was recorded in real-time using RTCA Control Unit (Roche Applied Science, Switzerland) and analyzed by RTCA software based on the average results of recorded data.

### Flow cytometry

About  $1 \times 10^6$  cells of HT29 were cultured in 2 ml of RPMI medium and grown 24 h before addition of paclitaxel, either as a water-soluble form or as paclitaxel-SA1-cetuximab. The concentration of both PY79 and SA1-cetuximab was  $1 \times 10^7$  spores/2 ml medium and the concentration of paclitaxel was 64 nM and paclitaxel-SA1-cetuximab was 16 nM. The negative controls were the cells without paclitaxel. The cells after 18 h incubation with paclitaxel and paclitaxel-SA1-cetuximab were collected and fixed by ethanol formaldehyde before

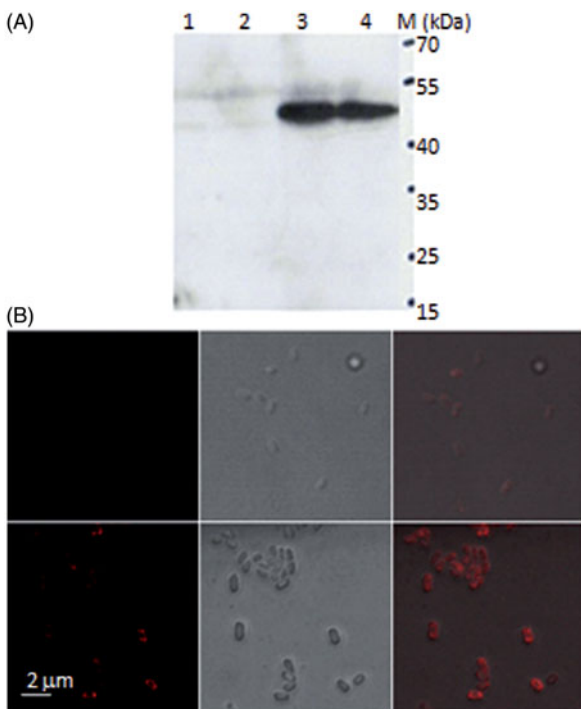


Figure 2. Expression of CotB-SA on the *B. subtilis* outer spore coat. Panel A: coat proteins were extracted from spores ( $2 \times 10^8$ ) of wild-type PY79 (lanes 1 and 2) and two SA1 isolates carrying the recombinant CotB-SA gene (lanes 3 and 4). The SA chimeric protein was detected using an anti-SA polyclonal antibody (Sigma-Aldrich, NY). Panel B: laser scanning confocal micrographs showing individual PY79 (upper images) and SA1 spores (lower images) labeled with anti-SA and secondary, anti-rabbit, antibodies conjugated with Alexa 546 as indicated by red signals (left panel) under excitation by green laser. The middle panel shows images of spores under white light. The right panel is a merged image of the left and middle panels. For interpretation of the references to color in this figure legend, the reader is referred to the web version of the article.

staining with PI (Propidium iodide) fluorescent dye 1  $\mu\text{g}/\text{ml}$  in PBS containing 10  $\mu\text{g}/\text{ml}$  RNase A at 37 °C, 30 min. The DNA content of stained cells was analyzed using an FACS Canto (Becton Dickinson, Germany). The analysis was repeated three times.

## Results

### Expression of CotB-SA on the surface of *B. subtilis* spores

A recombinant strain of *B. subtilis* named SA1 was constructed that carried a chimeric CotB-SA gene, CotB-SA, where CotB spore coat protein gene had been fused to the SA gene. Western blotting of the spore coat protein fractions revealed the presence of a protein species that reacted with SA-specific antibodies (Figure 2A, lanes 3 and 4). At about 50 kDa, this band was compatible to the theoretical size of the CotB-SA chimera (CotB, 35 kDa; monovalent SA 15 kDa). No band was detectable in spores of PY79 (the isogenic *B. subtilis* strain used for cloning) confirming the specificity of antigen–antibody interaction. SA1 spores expressing CotB-SA were specifically stained with anti-SA polyclonal rabbit IgG, followed by anti-rabbit IgG and labeled with the fluorescent dye Alexa 546, as indicated by clear red signals on individual spores of SA1 (Figure 2B, lower images).

Background signals due to non-specific interaction between antibodies and coat proteins were extremely low in *B. subtilis* PY79 (Figure 2B, upper images). This shows that SA can be expressed on the spore surface and retains its integrity.

### Binding affinity and pH stability of biotinylated cetuximab to killed spores expressing SA

SA1 spores ( $1 \times 10^9$ ) were firstly killed by autoclaving, and then tested for binding with cetuximab, an inhibitor of EGFR. Biotinylated anti-EGFR monoclonal IgG (cetuximab) at 1  $\mu\text{g}$  was bound to spores. The unbound cetuximab was washed off and then  $2 \times 10^8$  cetuximab bound SA1 spores were examined by SDS-PAGE fractionation and Western blotting (Figure 3A). The DTT in the SDS-PAGE loading buffer would reduce the disulfide bridge of IgG, resulting in two fragments corresponding to the light and heavy chains. We could clearly observe a band of about 60 kDa indicating the size of cetuximab which was bound to the spores (Figure 3A, lane 1). The intensity of this band was equal to 45% intensity of the control 100 ng biotinylated cetuximab (Figure 3A, lane 3), indicating that the amount of cetuximab bound on  $2 \times 10^8$  SA1 spores was about 45 ng, which implied that about 225 ng from the 1  $\mu\text{g}$  of incubated cetuximab had bound to  $1 \times 10^9$  SA1 spores. On the other hand, PY79 did not show any observable band (Figure 3A, lane 2) demonstrating specific binding of biotinylated cetuximab to the SA expressed as a fusion protein with CotB on the spores. We next verified the binding constants of biotinylated cetuximab to SA1 based on an equation (as described in the “Materials and methods” section) and which was used to correlate binding cetuximab concentration against initial cetuximab concentration. As shown in Figure 3(B), the binding curve correlated well with the equation with an *R* value of  $\sim 0.94$ . The number of CotB-SA molecules per  $\mu\text{m}^2$  on a spore was  $3.7 \times 10^3$  and the binding constant ( $K_{S-C}$ ) between the SA1 on spores with biotinylated cetuximab was  $10^7 \text{ M}^{-1}$ . This binding was particularly stable since we obtained the same intensity of cetuximab bound on spores either at day 0 or after 7 days. This implied that the dissociation rate  $k_{off(S-C)}$  was fairly low and below  $6.87 \times 10^{-5} \text{ min}^{-1}$ . We further tested if this binding was stable at different pH, resembling the changing pH in the gastrointestinal tract. We found that binding was stable from pH 2 to pH 8 (Figure 3C, lanes 1–4) and reduced only to half at pH 10 (Figure 3C, lane 5). Therefore, we succeeded in creating a stable carrier (SA1 spores) that expressed SA and which could bind biotinylated cetuximab (we refer to this henceforth as SA1-cetuximab).

### Toxicity of killed SA1-cetuximab spores toward growth of HT29 and KPL4 cells

“Killed” SA1 spores ( $1 \times 10^8$  cfu), “killed” SA1-cetuximab spores ( $1 \times 10^8$  cfu) and cetuximab (20 ng) were added to individual wells containing 200  $\mu\text{l}$  medium to test whether they produced a defect in the normal growth of colon cancer cells using HT29 and breast cancer KPL4 cells. The final concentration of cetuximab in each well was calculated as 100 ng/ml, equivalent to 8.3 nM (since the molecular weight of cetuximab is 120 kDa). We performed real-time observation of cell growth as indicated by the cell index against

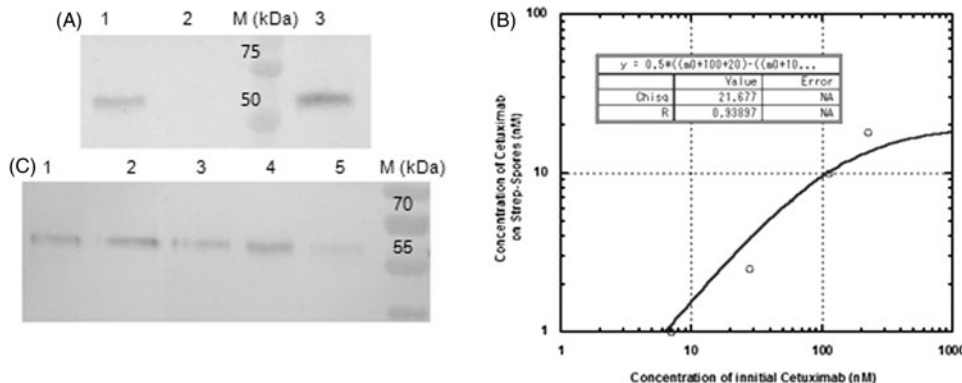


Figure 3. Western analysis of binding of biotinylated cetuximab to SA1 spores. Panel A: 1 µg of biotinylated mouse-human chimeric monoclonal IgG cetuximab was bound to  $1 \times 10^9$  killed spores (SA1, lane 1, and PY79, lane 2) and total extracted proteins of  $2 \times 10^8$  spores were applied to each well, and then were fractionated on 12% SDS-PAGE gels and transferred to membranes and probed with anti-human IgG conjugated with Alkaline Phosphatase (Promega, WI). A positive control was 100 ng biotinylated cetuximab applied directly to the well and run in parallel (lane 3). Molecular weight markers (kDa) are indicated. Panel B: 0.25 µg, 1 µg, 4 µg and 8 µg of biotinylated cetuximab was bound to  $1 \times 10^9$  killed spores and the biotinylated cetuximab bound to spores was plotted (circles). Panel C: binding of 1 µg biotinylated cetuximab to  $1 \times 10^9$  killed spores at different pH's, ranging from 2 (lane 1), 4 (lane 2), 6 (lane 3), 8 (lane 4), to 10 (lane 5), and total proteins of  $2 \times 10^8$  spores were used for Western analysis. Molecular weight markers (kDa) are indicated.

time (see “Materials and methods” section). As shown in Figure 4(A), HT29 cells grew well in the presence of “killed” SA1-cetuximab (Figure 4A, circle gray line) at very high concentrations of  $10^8$  cfu/200 µl giving similar growth curve with the control HT29 cells only (Figure 4A, square dark-white line) while the SA1-cetuximab (Figure 4A, black diamond line) and medium (Figure 4A, black triangle line) did not contribute significantly to the index values. We also found that SA1 itself and cetuximab at high doses did not decrease the cell index value during the observation time (data not shown). Similar results were obtained in the case of KPL4 cells and they grew normally in the presence of high concentration of either SA1-cetuximab (Figure 4B), or SA1, cetuximab (data not shown). These results indicated that SA1-cetuximab was essentially harmless and did not impair growth of HT29 and KPL4, and so could be used in further experiments to test its ability as drug carrier to deliver paclitaxel toward HT29 and KPL4 cells.

### Adsorption of paclitaxel on killed SA1-cetuximab spores

SA1 and PY79 spores were incubated with dual-labeled biotinylated Alexa-546 cetuximab 20 nM and paclitaxel Oregon Green 488 (excitation/emission: 488 nm/525 nm) at 200 nM to show that SA1 and PY79 spores could adsorb paclitaxel. As shown in Figure 5(A), we could clearly observe green signals of similar intensity indicating that paclitaxel Oregon Green 488 bound to both types of spores at almost the same level. The green signal of SA1 (Figure 5A, lower image) merged completely with the red signal of Alexa 546 labeled cetuximab (Figure 5B, lower image), indicating that the adsorption of paclitaxel onto the SA1-cetuximab spores (Figure 5C). In the case of PY79 spores, the red signal of Alexa-546 was too dim to observe (Figure 5B, lower image), confirming the specificity of the CotB-SA with the biotinylated cetuximab. We could see that after binding with cetuximab and paclitaxel, the ellipsoidal shape and size of SA1 was significantly unchanged, and was of the same size as

wild-type PY79. SA1-cetuximab spores were evaluated as a carrier of paclitaxel at different spore concentrations. Adsorption of paclitaxel on  $1 \times 10^8$  SA1-cetuximab spores was quantitatively measured in comparison to  $1 \times 10^8$  spores of the wild-type non-recombinant *B. subtilis* isogenic strain PY79 by fluorescence spectrofluorimetry, with paclitaxel Oregon Green 488 concentrations ranging from 200 nM to 1 µM. As shown in Figure 5(D), adsorption of paclitaxel on both types of spores also increased in parallel with the increasing concentration of paclitaxel, accumulating 50% binding at around 625 nM, indicating that the dissociation constant  $K_d$  was 625 nM. From this  $K_d$  value measured in 1 ml buffer, we can estimate that  $10^8$  SA1-cetuximab spores adsorbed about 1.25 ng paclitaxel, equivalent to  $10^{12}$  spores carrying 12.5 mg paclitaxel. At 1 µM initial paclitaxel concentration about 800 nM paclitaxel was adsorbed onto spores. The binding was stable in PBS buffer for more than 48 h at different pH values ranging from 2 to 8. In the human serum, the binding was also stable even for 48 h. These data imply that the dissociation rate of adsorption  $k_{off(P-SA1-cetuximab)}$  in both PBS and the serum was below  $2.4 \times 10^{-5} \text{ min}^{-1}$ .

### Enhanced binding of paclitaxel to HT29 colon cancer cells when delivered by SA1-cetuximab

We further evaluated the binding of paclitaxel using delivery by SA1-cetuximab, in comparison to that of water-soluble paclitaxel and paclitaxel adsorbed on wild-type *B. subtilis* PY79. After 4 h incubation using three formulations of paclitaxel with HT29 colon cancer cells, it was found (Figure 6) that water-soluble paclitaxel could bind to HT29 cells but was only clearly observable in about 3% of the cell population as indicated by a green signal (Figure 6B). In control experiments, HT29 cells without paclitaxel incubation showed only a blue signal of DAPI staining the nucleus, without an observable green signal. Paclitaxel bound on wild-type *B. subtilis* PY79 also showed low but clear green signals of binding in about 4% of cells even though most of paclitaxel

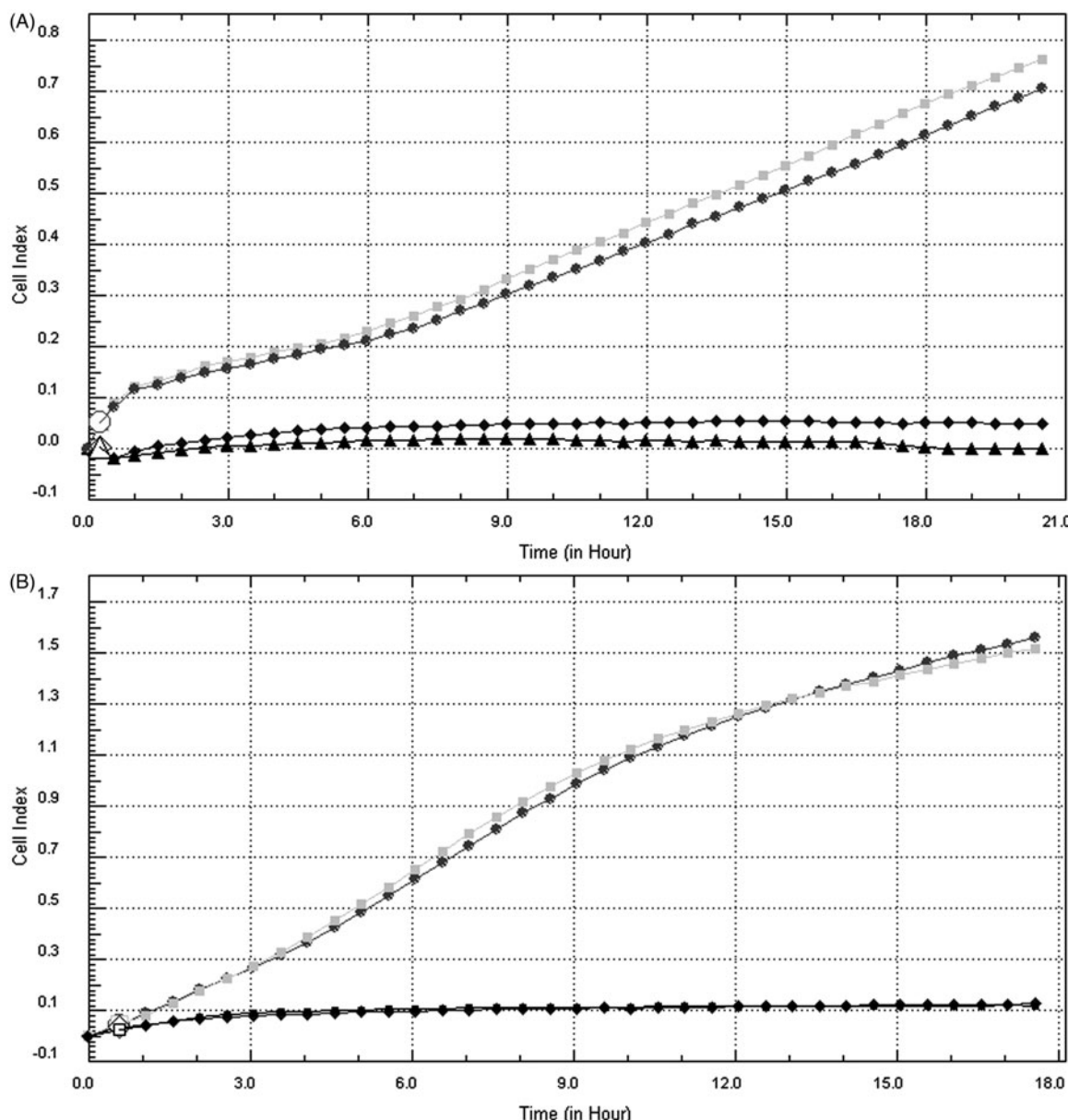


Figure 4. Real-time monitoring of HT29 and KPL4 growth without and with the presence of SA1-cetuximab. Panel A: averaged real-time curves of cell index of HT29 only (■), 10 000 HT29 cells mixed with  $1 \times 10^8$  SA1-cetuximab spores (●), medium (▲) and  $1 \times 10^8$  SA1-cetuximab (◆). Panel B: averaged real-time curves of cell index of KPL4 only (■), 2000 KPL4 cells mixed with  $1 \times 10^8$  SA1-cetuximab spores (●), medium (▲), and SA1-cetuximab (◆).

remained on the spores bound to the surface of HT29 cells (Figure 6C). Interestingly, when paclitaxel was delivered by SA1-cetuximab, the intensity of paclitaxel bound to HT29 cells was increased significantly with almost all cells labeled green (Figure 6D). When the concentration of paclitaxel-SA1-cetuximab was lowered to 250 nM, we also observed a similar intensity to that of water-soluble paclitaxel at 1  $\mu$ M (data not shown). These results indicate that a 4-fold enhancement in binding of paclitaxel to HT29 colon cancer cells was obtained when paclitaxel was delivered by SA1-cetuximab. To test the specificity of SA1-cetuximab for delivery of paclitaxel to HT29 colon cancer cells, we performed similar experiments with the KPL4 breast cancer cells, which was a cetuximab-resistant cell line. In fact, the control KPL4 cells without incubation of paclitaxel emitted only faint green signals of autofluorescence. As shown in Figure 6(E), after setting an off-set to remove the

background signal, we observed only the blue signal (nucleus). In Figure 6(H), the intensity of clear green signals indicating binding of paclitaxel Green Oregon 488 in KPL4 cells when incubated with 1  $\mu$ M paclitaxel-SA1-cetuximab was marginally higher than that with 1  $\mu$ M of the water-soluble form (Figure 6F) and was almost equal to that with 1  $\mu$ M paclitaxel-PY79 (Figure 6G). In conclusion, SA1-cetuximab spores delivered paclitaxel more specifically and efficiently to the target colon cells than unmodified PY79 spores.

#### Paclitaxel-SA1-cetuximab inhibits growth of HT29

Since SA1-cetuximab delivered paclitaxel more specifically to the target HT29 cells compared to the water-soluble paclitaxel, we asked whether this targeted delivery could augment inhibition of cell growth. The growth of cells in the

Figure 5. Adsorption of paclitaxel labeled Oregon to SA1spores bound with biotinylated cetuximab labeled Alexa 546. Panels A and B: laser scanning confocal micrographs showing individual spores from the PY79 (upper images) and SA1 (lower images) adsorbed with paclitaxel-Oregon (Panel A, green signal) and bound with cetuximab doubly biotinylated and labeled with Alexa546 (Panel B, red signal). Panel C is a merged image of Panel A and Panel B. Panel D: fluorospectrometry of Oregon Green 488 emission showing the plots of binding paclitaxel (vertical axis) against the initial incubated paclitaxel (horizontal axis) on the wild-type PY79 (red color, □) and on SA1-cetuximab (light blue color, ◇). At four values of  $P_0$  ranging from 200 nM to 1  $\mu$ M, the relative  $P_b$  was measured at a concentration of  $1 \times 10^8$  spores/ml. The error bars were too small to be recognized by the naked eye. For interpretation of the references to color in this figure legend, the reader is referred to the web version of the article.

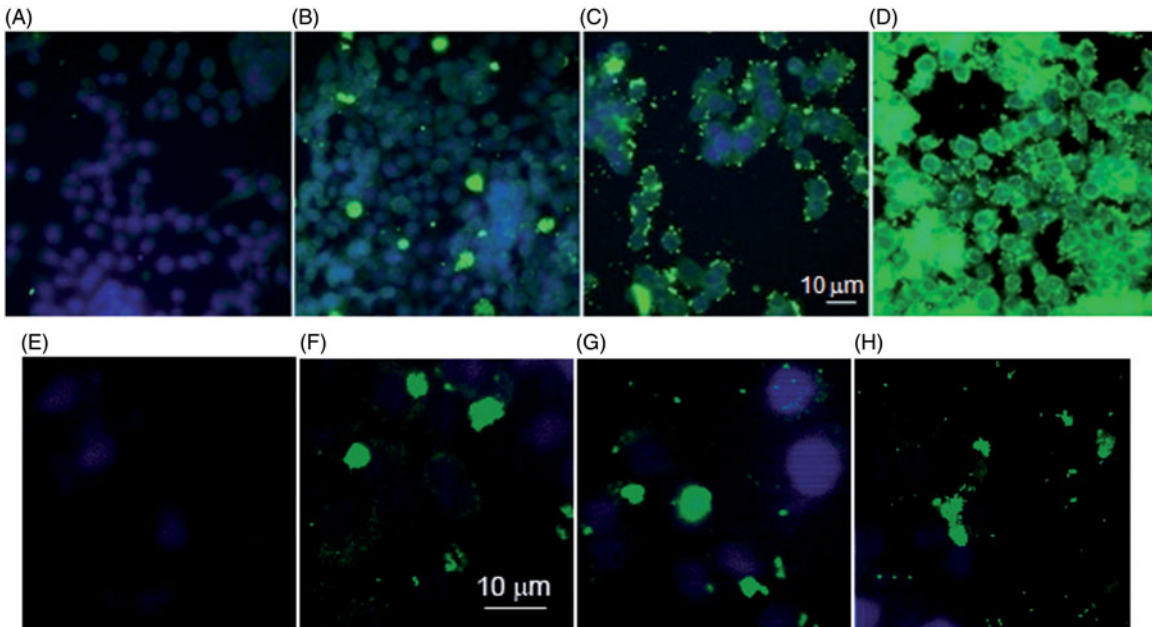
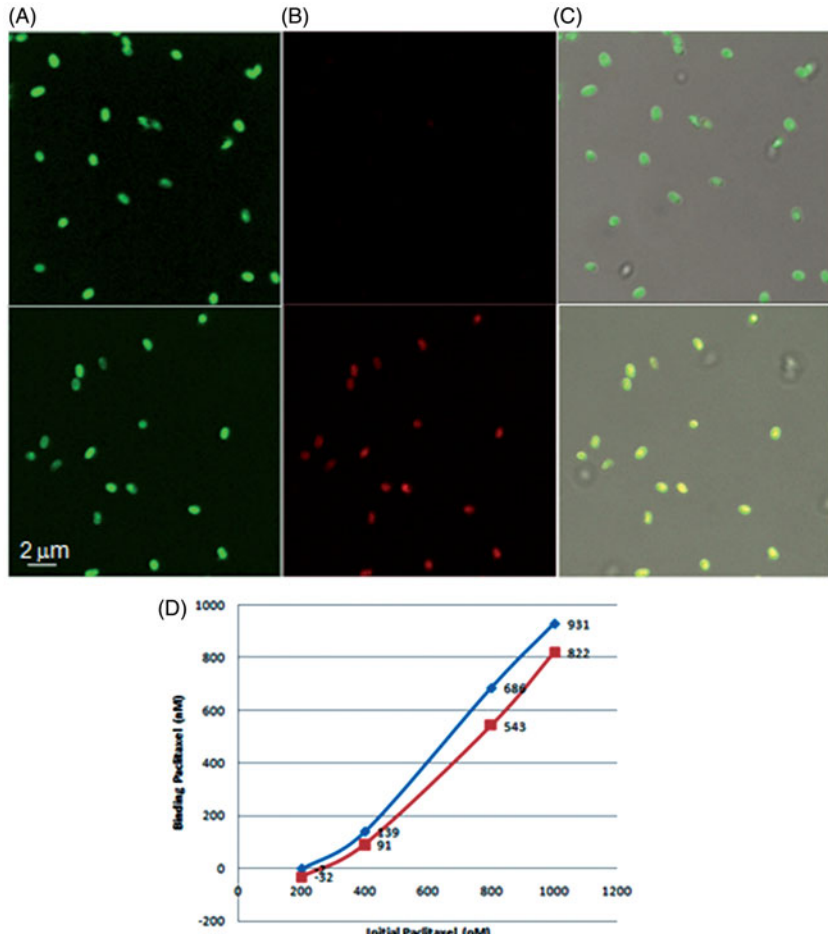


Figure 6. Binding of paclitaxel labeled Oregon on HT29 colon cancer cells and KPL4 breast cancer cells. Laser scanning confocal micrographs showing the green signal of paclitaxel Oregon 488 bound on HT29 cells and KPL4 cells at concentrations of 1  $\mu$ M paclitaxel in different formulations. Upper panels for HT29. Negative control image without paclitaxel (panel A), water-soluble paclitaxel (panel B), paclitaxel adsorbed to  $5 \times 10^8$  spores of PY79 (panel C), paclitaxel adsorbed with  $5 \times 10^8$  SA1 spores (panel D). Lower panels for KPL4. Negative control image without paclitaxel (panel E), water-soluble paclitaxel (panel F), paclitaxel adsorbed to  $5 \times 10^8$  spores of PY79 (panel G), and paclitaxel adsorbed to  $5 \times 10^8$  spores of SA1-cetuximab (panel H). For interpretation of the references to color in this figure legend, the reader is referred to the web version of the article.

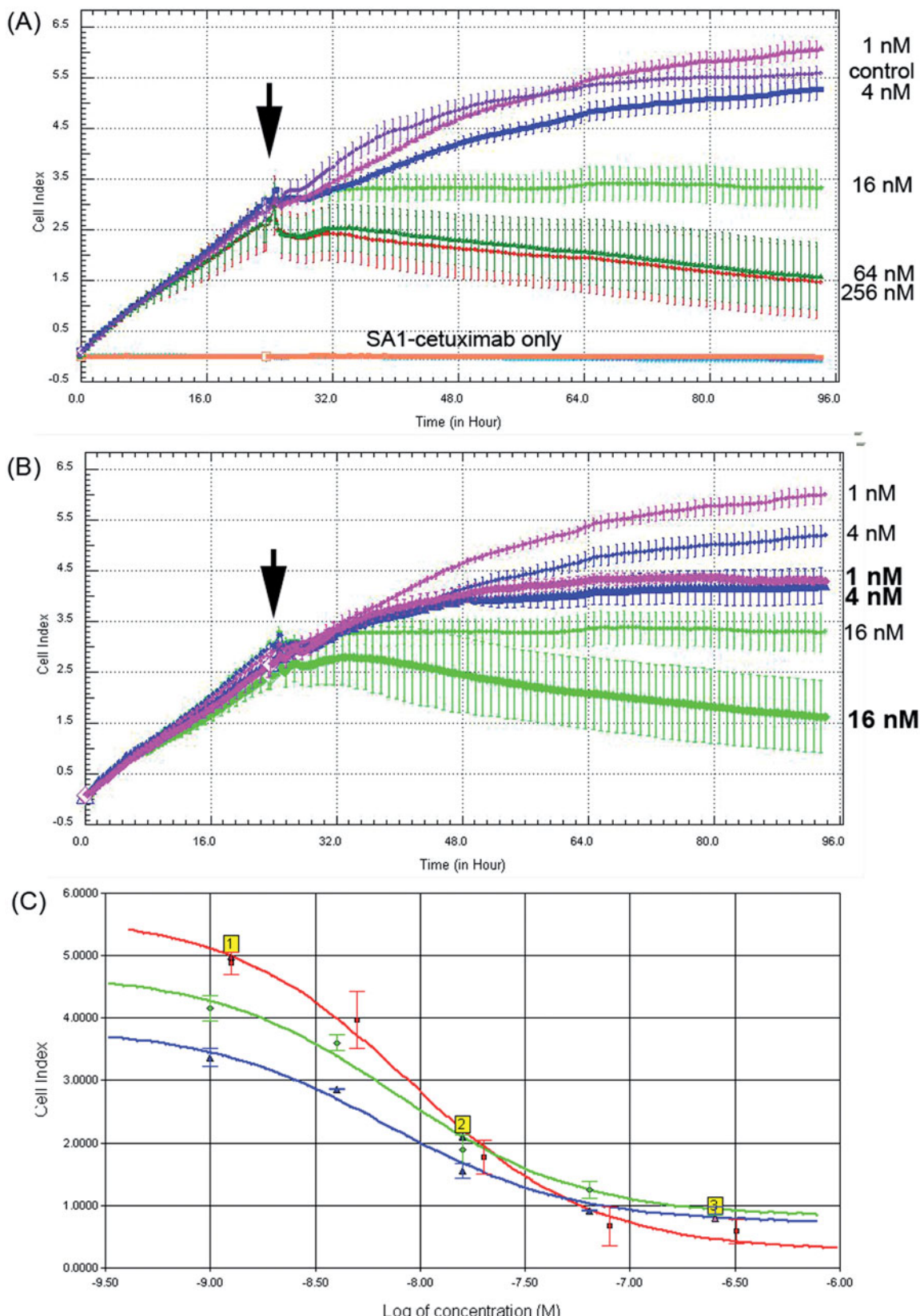


Figure 7. Inhibition of HT29 cell growth by paclitaxel. Real-time monitoring of growth of 10 000 HT29 cells upon addition of water-soluble paclitaxel and different concentrations ranging from 1 nM to 1  $\mu$ M and in comparison to paclitaxel-PY79 and paclitaxel-SA1-cetuximab. Panel A: averaged real-time curves of cell index for water-soluble paclitaxel at 1 nM (magenta), 4 nM (blue), 16 nM (green), 64 nM (red) and 256 nM (dark green). Controls were HT29 only (violet, control), medium, PY79 and SA1-cetuximab only (orange). Vertical bars indicate errors of triplicate samples. An arrow indicates the start of paclitaxel addition. Panel B: averaged real-time curves of cell index for water-soluble paclitaxel at 1 nM (bold letter, thick magenta), 4 nM (bold letter, thick blue) and 16 nM (bold letter, thick green). Vertical bars indicate errors of triplicate samples. An arrow indicates the beginning of adding paclitaxel. Panel C: averaged curves of cell index plotted against concentration of water-soluble paclitaxel (line 1, red), paclitaxel-PY79 spore (line 2, green) and paclitaxel-SA1-cetuximab (line 3, blue) to calculate  $IC_{50}$ . For interpretation of the references to color in this figure legend, the reader is referred to the web version of the article.

presence of water-soluble paclitaxel or paclitaxel-SA1-cetuximab was recorded in a real-time profile (Figure 7). At 1 nM paclitaxel (Figure 7A, magenta thin line) the growth of cells was almost normal and the same as when paclitaxel was not added (Figure 7A, blue violet thin line). As controls, we found that either  $1 \times 10^6$  SA1-cetuximab spores (containing  $\sim 0.2$  ng cetuximab), PY79 ( $1 \times 10^6$  PY79 spores), or cetuximab (up to 20 ng, 100-fold higher amount compared to that of cetuximab bound on SA1) did not cause any defect in cell growth in the 200  $\mu$ l well. At increasing concentrations from 4 nM to 64 nM of paclitaxel added to cells (as indicated by an arrow), the growth of cells was inhibited at increasing levels as shown in Figure 7(A). In detail, at 64 nM (Figure 7A, dark green line) the inhibition of growth was the same as that at 256 nM (Figure 7A, red line) and 1  $\mu$ M (data not shown), indicating the saturation of cell-growth inhibition was obtained at 64 nM, and that reliability in paclitaxel concentrations for electric measurement of cell growth inhibition was within 1–64 nM. When we used the paclitaxel-SA1-cetuximab at the same concentration ranging from 1 nM to 16 nM, we always obtained a higher level of cell growth inhibition as indicated by the thick lines, in comparison to that as indicated by the thin lines for water-soluble paclitaxel (Figure 7B). Specifically, the level of inhibition of cell growth at 1 nM paclitaxel-SA1-cetuximab (Figure 7B, bold letter, thick magenta line) was much stronger than that at 1 nM and even at 4 nM water-soluble paclitaxel (Figure 7B, magenta and blue thin lines). When paclitaxel-SA1-cetuximab was increased to 16 nM, the inhibition curve (Figure 7B, bold letter, thick green line) was similar to that at 64 nM water-soluble paclitaxel (Figure 7A, thin green line). When we compared the  $IC_{50}$  of paclitaxel at different formulations, either in water-soluble form or paclitaxel adsorbed on PY79 or SA1-cetuximab (Figure 7C), we realized that the  $IC_{50}$  of paclitaxel-SA1-cetuximab was much lower (2.9 nM) than that of the  $IC_{50}$  of paclitaxel-PY79 (7.8 nM) and the  $IC_{50}$  of water-soluble paclitaxel (14.5 nM). These data confirm an approximate 5-fold enhancement of HT29 cell inhibition when paclitaxel is delivered by SA1-cetuximab. The specificity in paclitaxel-delivery by SA1-cetuximab was again shown by performing cell-growth inhibition of KPL4 using water-soluble paclitaxel and paclitaxel-SA1-cetuximab at concentrations ranging from 1 nM to 64 nM, at which reliability of detection was obtained (Figure 8A). In fact, we observed similar cell growth curves as demonstrated at 4 nM of paclitaxel (Figure 8A, blue line) and 4 nM paclitaxel-SA1-cetuximab (Figure 8A, bold letter, cyan line). The  $IC_{50}$  in this case was determined to be 2.3 nM for water-soluble paclitaxel and 1.5 nM for paclitaxel-SA1-cetuximab (Figure 8B), indicating that the enhancement of KPL4 cell inhibition was only 1.5-fold when paclitaxel was delivered by SA1-cetuximab.

### Enhanced inhibition of cell division by paclitaxel-SA1-cetuximab

When we compared the DNA content of HT29 before and after treatment with different concentrations of water-soluble paclitaxel and paclitaxel-SA1-cetuximab at 16 nM and 64 nM, we found that the DNA content profile of HT29

when treated with 16 nM water-soluble paclitaxel (Figure 9A) was not substantially different from that of HT29 before treatment (Figure 9B). In both cases, the population of apoptotic nuclei represented by a sub-diploid peak was only 7%, the diploid nuclei population was abundant (51%) and polyploidy nuclei population was about 32%. When HT29 was treated with paclitaxel-SA1-cetuximab at this concentration, the DNA content of cells became more unstable, resulting in a more abundant (50.6%) population of polyploidy cells (Figure 9D). These data indicate that a population of 20% cells has either stopped at G1 phase after tripolar mitosis or entered mitotic slippage when paclitaxel was delivered by SA1-cetuximab. Nevertheless, when cells were treated with 64 nM water-soluble paclitaxel, the polyploidy population was increased to 74.2% (Figure 9C), indicating that the instability of DNA content was obviously enhanced 2-fold, but less than 4-fold when paclitaxel was delivered by SA1-cetuximab within 18 h.

### Discussion

In terms of targeting cancer cells, spores can be genetically engineered to express proteins to target specific biomarkers to the membranes of cancer cells. However, for safety in use of genetically modified organism for application as a drug carrier, spores must be killed to avoid germination and release into the environment. To deliver drugs to colon cancer cells, the autoclaved recombinant spores expressing CotB-SA were used to specifically interact with biotinylated cetuximab that could target cetuximab-sensitive colon cancer cells. The created cetuximab-bound spores were for the first time tested to adsorb and deliver paclitaxel, a common chemical in cancer treatment, into the colon cells.

In this seminal study, SA has been successfully expressed as a fusion protein with CotB on the outer coat of *B. subtilis* spores PY79 and tested for delivery paclitaxel to colon cancer cells. The number of SA molecules on a  $\mu\text{m}^2$  of a single spore is about  $3.7 \times 10^3$ , meaning there was a probability of about 0.04 molecules per  $10 \text{ nm}^2$  area which was the average two-dimensional size of a 50 kDa protein ( $3.3 \text{ nm} \times 3.3 \text{ nm}$ ). This number indicates somewhat low expression of “active” SA molecules and that there is still a significant “gap” between individual SA molecules on the outer surface of spores, so that “side-by-side” interaction of multi-SA molecules was not achieved here as expected for the classical model of binding of biotin to tetrameric SA. Although, the measured binding affinity  $K_{S-C}$  was 7-fold lower than the best  $K_b = 7 \times 10^7$  for monovalent SA to biotin (mutant T90A/D128A SA exists as monomer) which has been reported by Qureshi and Wong in 2002 [19], this  $K_{S-C}$  was comparable to constants of antigen–antibody interaction, normally ranging from  $10^7 \text{ M}^{-1}$  to  $10^9 \text{ M}^{-1}$ . And most importantly, the dissociation rate of biotinylated cetuximab from SA1 was extremely slow and the binding was even stable within two months, ensuring delivery of paclitaxel bound on SA1 to target cells as this process required only 6 h as shown in Figure 6 (Panel D). Taken together, it is possible to conclude that SA expressed as a fusion protein with CotB on the surface of killed *B. subtilis* spores can interact specifically and stably with biotinylated cetuximab.

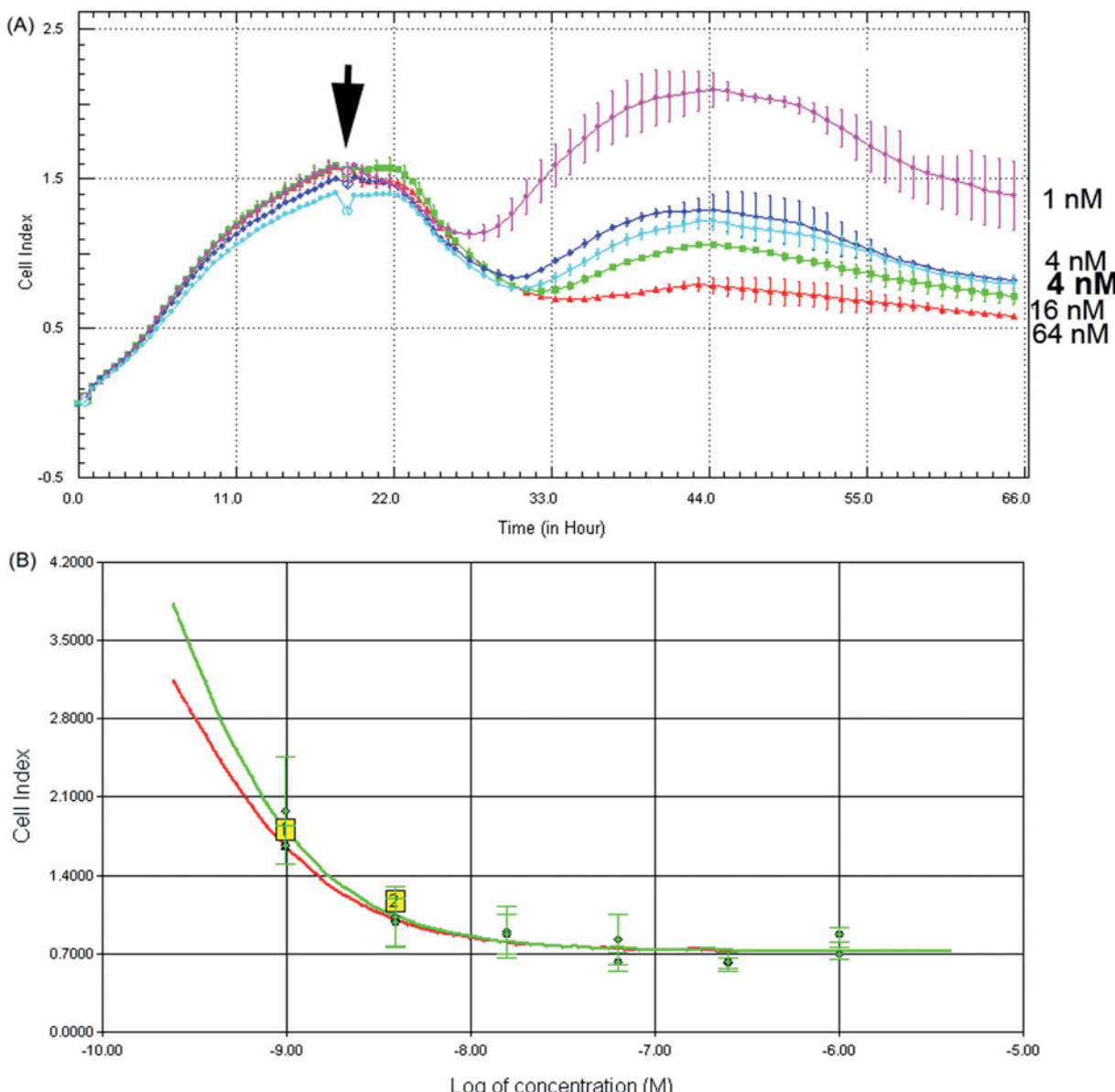
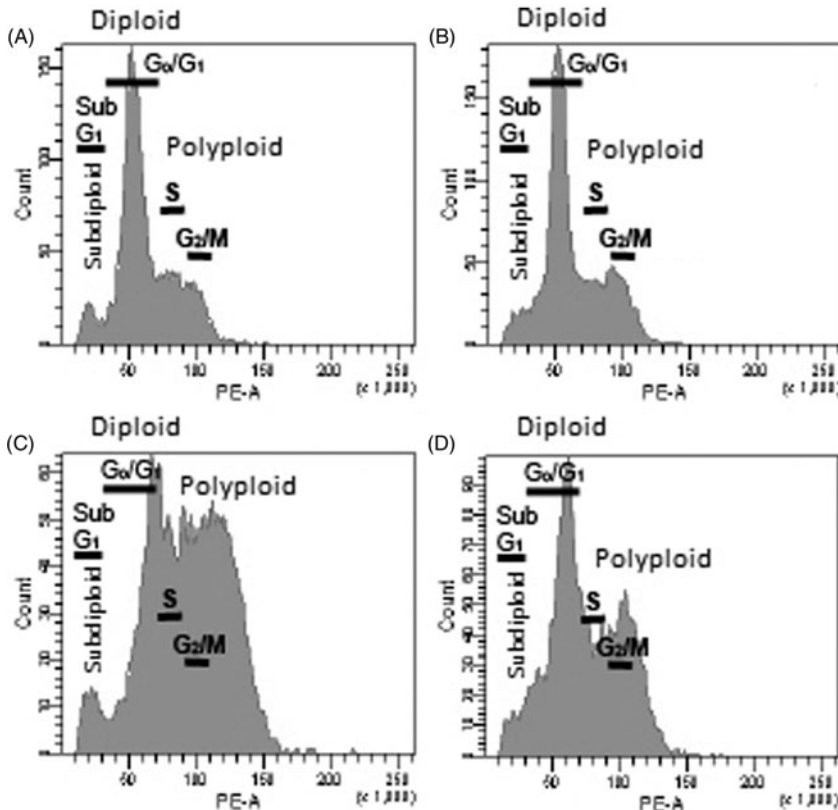


Figure 8. Inhibition of KPL4 cell growth by paclitaxel. Real-time monitoring of growth inhibition of 2000 KPL4 cells upon addition of water-soluble paclitaxel at different concentrations ranging from 1 nM to 1  $\mu$ M and in comparison to paclitaxel-SA1-cetuximab. Panel A: averaged real-time curves of the cell index for water-soluble paclitaxel at 1 nM (magenta), 4 nM (blue), 16 nM (green), 64 nM (red) and paclitaxel-SA1-cetuximab at 4 nM (bold letter, cyan). An arrow indicates the beginning of adding paclitaxel. Panel B: averaged curves of cell index plotted against concentration of water-soluble paclitaxel (line 1, red) and paclitaxel-SA1-cetuximab (line 2, green) to calculate IC<sub>50</sub>. For interpretation of the references to color in this figure legend, the reader is referred to the web version of the article.

For the purpose of delivery of anti-cancer reagents using SA1-cetuximab to target cells, SA1-cetuximab has been tested for its toxicity toward growth of two cancer cell lines, including colon cancer cell HT29 over-expressing EGFR biomarker and the breast cancer cell line KPL4 which under expresses the EGFR biomarker. The data in Figure 4 prove that SA1-cetuximab, even at very high concentration ( $1 \times 10^8$  spores/well, 100-fold higher than the dose used as drug-carrier), is completely non-toxic to both cell lines. The cetuximab concentration used in the toxicity assay (100 ng/ml,  $\sim 8.3$  nM) was about 100-fold higher than the dose used as a drug-carrier SA1-cetuximab (1 ng/ml,  $\sim 0.08$  nM), but still was 100-fold lower than the dose (10  $\mu$ g/ml,  $\sim 830$  nM) which has been reported to inhibit 30% cell proliferation of HT29 [37]. SA1-cetuximab must

therefore function as an adjuvant for therapeutic reagents. Here we intentionally used paclitaxel as it will adsorb well onto the hydrophobic surface of SA1 spores. We required stable adsorption of paclitaxel within about 6 h to guarantee almost all adsorbed paclitaxel could reach the target cells. However, the binding affinity of paclitaxel to SA1-cetuximab spores must be weaker than that of paclitaxel to microtubules so that the association could be switched to favor paclitaxel-microtuble binding, enabling cell division to be interrupted. To visualize paclitaxel's binding on the spores and to track localization of paclitaxel in HT29 cells, we must use fluorescent-labeled paclitaxel Oregon Green 488. Oregon Green 488 is hydrophilic probe which does not interfere or change the hydrophobicity of paclitaxel, thus the paclitaxel-Oregon Green 488 closely reflects the character of non-

Figure 9. Effect of paclitaxel and paclitaxel-SA1-cetuximab DNA-content of HT29 cells. Flow cytometric analysis of HT29 cell populations having different DNA content profiles as indicated by the intensity of the DNA-specific fluorescent dye PI (PE-A). Panel A: populations of sub-diploid cells (7.6%), diploid cells (60.9%) and polyploidy cells (32.6%) in control HT29 without treatment of paclitaxel. Panel B: populations of sub-diploid cells (7.1%), diploid cells (62.9%), and polyploidy cells (31.5%) in HT29 treated with 16 nM paclitaxel. Panel C: populations of sub-diploid cells (5.1%), diploid cells (22.4%), and polyploidy cells (74.2%) in HT29 cells treated with 64 nM paclitaxel. Panel D: populations of sub-diploid cells (6.9%), diploid cells (44.5%), and polyploidy cells (50.6%) in HT29 treated with 16 nM paclitaxel-SA1-cetuximab.



labeled paclitaxel. Our observation in Figure 5 indicates that the shape and size of SA1-cetuximab-paclitaxel is significantly unchanged compared to either SA1 or wild-type PY79 spores. The ellipsoidal dimensions of *B. subtilis* PY79 spores have been measured to be about 600 nm × 900 nm by Huynh and her colleagues using transmission electron microscopy [38], and these are therefore much larger than the size of conventional nanoparticles, typically less than 100 nm. Instead, the binding capacity for antibodies and/or various chemical moieties (e.g. paclitaxel) of our spores is much greater than that of conventional nanoparticles, and the increase in spherical dimension of the spores after binding with cetuximab and paclitaxel is negligible. Additionally, as shown in Figure 5, the stability and uniformity of our spores are much greater than that of conventional nanoparticles.

The dissociation rate for paclitaxel-Oregon from SA1-cetuximab in both PBS (at different pH) and even in the serum was quite slow, as indicated by the half-life which was greater than 48 h. This value was much longer than that required for paclitaxel to reach the target cells, thus we believe that almost all adsorbed paclitaxel was likely to be delivered to the HT29 colon cancer cells, and that paclitaxel could target colon cancer tumors if tested in an *in vivo* model. This might result from the highly hydrophobic character of the outer layer of PY79 spores which could promote tight binding between paclitaxel and the outer layer of PY79 spores. As shown in Figure 6(C), paclitaxel could also bind to *B. subtilis* wild-type PY79 spores attached to surrounding HT29 cells. However, we observed a low intensity of paclitaxel inside the HT29 cells, indicating that paclitaxel could not enter the cells efficiently even though it was brought in close contact with the cell membranes. By contrast, the high intensity of paclitaxel Oregon Green 488 in Figure

6(D) suggests that SA1-cetuximab not only delivers paclitaxel to HT29 cell membranes, but may also enter the cells through endocytosis via specific interaction between cetuximab and EGFR. However, to prove specificity in the “SA1-cetuximab-EGFR” models, further experiments of knock-down expression of EGFR levels in HT29 cell line should be performed. The 4-fold increasing intensity of paclitaxel Oregon Green 488 inside the HT29 cells when paclitaxel is adsorbed on SA1-cetuximab has proven the specificity of delivery. The dissociation constant ( $K_d$ ) of paclitaxel from SA1 spores was about 625 nM which was about 10-fold weaker than that ( $K_d \sim 60$  nM) of paclitaxel-microtubules [39]. Therefore, if paclitaxel-SA1-cetuximab could enter the cells, the association direction could be switched toward paclitaxel-microtubules. We propose this hypothetical model for delivery of paclitaxel to HT29 colon cancer cells by SA1-cetuximab in Figure 10.

The 4-fold enhancement in binding of paclitaxel to HT29 cells (Figure 6D) was almost in agreement with the 5-fold reduction in value of  $IC_{50}$  (Figure 7C), suggesting that the DNA instability or inhibition in cell division should be increased within a range of about 4- to 5-fold. However, we obtained only a 2-fold increase in the population of polyploidy nucleic cells using a treatment of 16 nM paclitaxel-SA1-cetuximab compared to that of 16 nM water soluble paclitaxel (Figure 9B and D). This population was less abundant to that in the case of 64 nM water-soluble paclitaxel (Figure 9C), indicating that the DNA instability has not yet increased to 4- or 5-fold and was similar to our data for cell growth inhibition. This difference could be explained due to the different observation times, 72 h in case of cell growth inhibition, and only 18 h in the case of DNA content analysis. Re-examination of the inhibition of cell growth at 18 h after

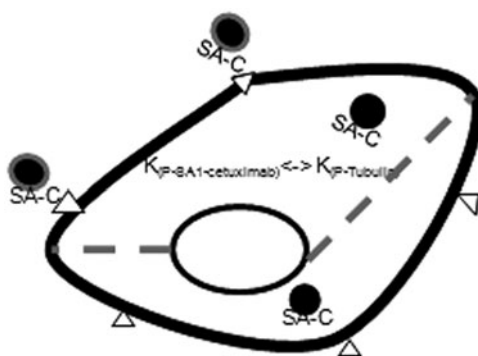


Figure 10. Model for SA1-cetuximab as anti-cancer chemicals for target cancer cells. A complex of spores expressing CotB-SA conjugated with biotinylated antibody (SA1-C) and adsorbed with anti-cancer chemicals (gray) target cancer cells through specific interactions between antibody (C) and biomarkers (triangle) on the cancer cell's surface. The complex can enter the cell possibly due to endocytosis. Release of chemicals from the spores toward microtubules depends on the competition between the dissociation constants of paclitaxel-SA1-cetuximab  $k_{(P-SA1-C)}$  and paclitaxel-tubulin  $k_{(P-Tubulin)}$ .

the addition of paclitaxel as presented in the green curve of Figure 7(B) shows that the level of inhibition by 16 nM paclitaxel-SA1-cetuximab was only 2-fold higher than water-soluble paclitaxel. These data indicate that the time required for all paclitaxel to release from spores to be more than 18 h. It is impossible to measure  $k_{off}$  rate of paclitaxel released from spores when paclitaxel-SA1-cetuximab spores are inside the cells. However, with a dissociation rate of  $k_{off(P-SA1-cetuximab)}$  below  $2.4 \times 10^{-5} \text{ min}^{-1}$ , the release of paclitaxel from spores might be completed in 72 h.

In experiments with the cetuximab-sensitive HT29 cell line, we always performed parallel controls with a cetuximab-resistant breast cancer KPL4 cell lines having a lower level of EGFR expression for comparison of the specificity of targeting. As shown in Figure 6(F) and (G), we could see that the SA1-cetuximab did not substantially enhance the delivery of paclitaxel into KPL4, resulting in almost no change in cell-growth inhibition activity compared to using water-soluble paclitaxel.

Our calculation based on the data presented in Figure 5(D) shows that  $10^{12}$  SA1-cetuximab spores could adsorb about 12.5 mg paclitaxel. Thus, if SA1-cetuximab spores can enhance the cell-growth inhibition up to 5-fold (Figure 7), the conventional daily infusion dose of 75 mg paclitaxel for cancer patient could be reduced by 15 mg, which would require highly purified and condensed SA1-cetuximab spores at a level of  $\sim 1.2 \times 10^{12} \text{ cfu/g}$ . The binding of cetuximab onto SA1 spores is stable in a wide range of pH, and absorption of paclitaxel on the SA1-cetuximab spores was pH-independent, suggesting that spores could be used to deliver drugs by oral administration. However, with the colon cancer tumors located deep inside the intestinal track, the killed SA1-cetuximab spores would need to be administered through conventional transfusion techniques. As paclitaxel is a hydrophobic organic molecule, the level and rate of releasing paclitaxel could be readjusted and improved by choosing suitable *Bacillus* strains having spores with less hydrophobicity and appropriate surface multi-layers more suitable for organic compound adsorption/release.

## Conclusion

This study demonstrates that killed *B. subtilis* PY79 spores expressing SA can conjugate to biotinylated monoclonal antibody cetuximab, and that the conjugation is stable at various pH's. This approach has a number of positive attributes. First, as spores are dead there is no possibility of spore germination and release of the SA moiety. Second, as recombinant spores are killed, potential issues regarding the use of live GMOs are removed and in essence killed spores should be considered as microparticles. Third, as a demonstrator of this technology, spores conjugated with biotinylated cetuximab showed an obvious capacity to adsorb paclitaxel on their surface and promote its release into targeted colon cancer cells with 5-fold reduction in the  $IC_{50}$  of cell growth inhibition due to a 4-fold increase in the interruption of cell division. Therefore, the kinetics of paclitaxel delivery to other colon cancer cell lines and tumors using SA1-cetuximab spores should be further studied.

## Acknowledgements

We thank Bui Thu Thuy, Phan Huong Trang, Bui Thi Ngoc Anh and Nguyen Dinh Thang (KLEPT, VNU University of Science, Vietnam) for technical assistance, Hoang Thi My Nhungh (KLEPT, VNU University of Science, Vietnam) and Hisashi Tadakuma (Graduate School of Frontier Science, The University of Tokyo) for useful discussions.

## Declaration of interest

The authors report no conflicts of interest. The authors alone are responsible for the content and writing of this article.

This work was supported by grants from the Vietnamese Ministry of Science and Technology – NAFOSTED (106.2011.02) and L'OREAL-UNESCO National Fellowship for Women in Science to N.T.V.A.

## References

- Ghosh P, Han G, De M, et al. Gold nanoparticles in delivery applications. *Adv Drug Deliv Rev* 2008;60:1307–15.
- Sun C, Lee JSH, Zhang M. Magnetic nanoparticles in MR imaging and drug delivery. *Adv Drug Deliv Rev* 2008;60:1252–65.
- Patel T, Zhou J, Piepmeyer J, Saltzman W. Polymeric nanoparticles for drug delivery to the central nervous system. *Adv Drug Deliv Rev* 2012;64:701–5.
- Jong WHD, Borm PJA. Drug delivery and nanoparticles: applications and hazards. *Int J Nanomed* 2008;3:133–49.
- Maletzki C, Gock M, Klier U, et al. Bacteriolytic therapy of experimental pancreatic carcinoma. *World J Gastroenterol* 2010;16: 3546–52.
- Theys J, Pennington O, Dubois L, et al. Repeated cycles of clostridium-directed enzyme prodrug therapy result in sustained antitumour effects in vivo. *Br J Cancer* 2006;95:1212–19.
- Liu SC, Ahn GO, Kioi M, et al. Optimized clostridium-directed enzyme prodrug therapy improves the antitumor activity of the novel DNA cross-linking agent PR-104. *Cancer Res* 2008;68: 7995–8003.
- Hong HA, Le HD, Cutting SM. The use of bacterial spore formers as probiotics. *FEMS Microbiol Rev* 2005;29:813–35.
- Huang JM, Huynh HA, Hoang TV, et al. Mucosal delivery of antigens using adsorption to bacterial spores. *Vaccine* 2010;28: 1021–30.
- Henriques AO, Moran Jr CP. Structure, assembly, and function of the spore surface layers. *Annu Rev Microbiol* 2007;61:555–88.
- Song M, Hong HA, Huang JM, et al. Killed *Bacillus subtilis* spores as a mucosal adjuvant for an H5N1. *Vaccine* 2012;22:3266–77.

12. Ricca E, Cutting SM. Emerging applications of bacterial spores in nanobiotechnology. *J Nanobiotechnol* 2003;1:6–16.
13. Le DH, Huynh HA, Fairweather N, et al. Bacterial spores as vaccine vehicles. *Infect Immun* 2003;71:2810–18.
14. Le DH, Huynh HA, Atkins HS, et al. Immunization against anthrax using *Bacillus subtilis* spores expressing the anthrax protective antigen. *Vaccine* 2006;25:346–55.
15. Cutting SM. Spores as oral vaccines. In: Ricca E, Henriques AO, Cutting SM, eds. *Bacterial spore formers: probiotics and emerging applications*. Norfolk: Horizon Bioscience Press; 2004: 201–6.
16. Mauriello EMF. Display of heterologous antigens on the *Bacillus subtilis* spore coat using CotC as a fusion partner. *Vaccine* 2004;22: 1177–87.
17. Kim LH, Lee CS, Kim BG. Spore-displayed streptavidin: a live diagnostic tool in biotechnology. *Biochem Biophys Res Commun* 2005;331:210–14.
18. Green NM. Avidin and streptavidin. *Methods Enzymol* 1990;84: 51–67.
19. Qureshi, MH, Wong SL. Design, production, and characterization of a monomeric streptavidin and its application for affinity purification of biotinylated proteins. *Protein Express Purification* 2002;25:409–15.
20. Wilchek M, Bayer EA, Livnah O. Essentials of biorecognition: the streptavidin–biotin system as a model for protein–protein and protein–ligand interaction. *Immunol Lett* 2006;103:27–32.
21. Mendelsohn J, Baselga J. The EGF receptor family as targets for cancer therapy. *Oncogene* 2000;19:6550–65.
22. Sanford D, Markowitz SD, Bertagnolli M. Molecular basis of colorectal cancer. *New Engl J Med* 2009;361:2449–60.
23. Jhawer M. PIK3CA mutation/PTEN expression status predicts response of colon cancer cells to the epidermal growth factor receptor inhibitor cetuximab. *Cancer Res* 2008;68:1953–61.
24. McKay JA, Murray LJ, Curran S. Evaluation of the epidermal growth factor receptor (EGFR) in colorectal tumours and lymph node metastases. *Eur J Cancer* 2002;38:2258–64.
25. Cunningham D, Humblet Y, Siena S, et al. Cetuximab monotherapy and cetuximab plus irinotecan in irinotecan-refractory metastatic colorectal cancer. *New Eng J Med* 2008;351:337–45.
26. Horwitz SB. Mechanism of action of taxol. *Trends Pharmacol Sci* 1992;13:134–6.
27. Sambrook J, Fritsch EF, Maniatis T. *Molecular cloning: a laboratory manual*. 2nd ed. Cold Spring Harbor (NY): Cold Spring Harbor Laboratory; 1989.
28. Cutting SM, Vander Horn PB. Genetic analysis. In: Harwood CR, Cutting SM, eds. *Molecular biological methods for Bacillus*. Chichester, UK: Wiley; 1990:27–74.
29. Iстicato R, Cangiano G, Tran HT, et al. Surface display of recombinant proteins on *Bacillus subtilis* spores. *J Bacteriol* 2001; 183:6294–301.
30. Nicholson WL, Setlow P. Sporulation, germination, and outgrowth. In: Harwood CR, Cutting SM, eds. *Molecular biological methods for Bacillus*. Sussex, UK: Wiley; 1990; 391–450.
31. Nguyen TVA, Kamio Y, Higuchi H. Single-molecule imaging of cooperative assembly of  $\gamma$ -hemolysin on erythrocyte membranes. *EMBO J* 2003;22:4968–79.
32. Nguyen HA, Nguyen TVA, Kamio Y, Higuchi H. Single-molecule environment-sensitive fluorophores inserted into cell membranes by staphylococcal  $\gamma$ -hemolysin. *Biochemistry* 2006;45: 2570–6.
33. Mariadason JM, Arango D, Qiuhu S, et al. Gene expression profiling-based prediction of response of colon carcinoma cells to 5-fluorouracil and camptothecin. *Cancer Res* 2003;63:8791–812.
34. Kurebayashi J, Otsuki T, Tang CK, et al. Isolation and characterization of a new human breast cancer cell line, KPL-4, expressing the Erb B family receptors and interleukin-6. *Br J Cancer* 1999;79: 707–17.
35. Fujimoto-Ouchi K, Sekiguchi F, Tanaka Y. Antitumor activity of combinations of anti-HER-2 antibody trastuzumab and oral fluoropyrimidines capecitabine/5'-dFUrD in human breast cancer models. *Cancer Chemother Pharmacol* 2002;49:211–16.
36. Tada H, Higuchi H, Watanabe TM, Ohuchi N. *In vivo* real-time tracking of single quantum dots conjugated with monoclonal anti-HER2 antibody in tumors of mice. *Cancer Res* 2007;67:1138–44.
37. Xu H, Yu Y, Marciniak D, et al. Epidermal growth factor receptor (EGFR)-related protein inhibits multiple members of the EGFR family in colon and breast cancer cells. *Mol Cancer Ther* 1989;4: 435–42.
38. Huynh H, To E, Fakhry S, et al. Defining the natural habitat of *Bacillus* spore-formers. *Res Microbiol* 2009;160:134–43.
39. Li Y, Edsall Jr R, Jagtap PG, et al. Equilibrium studies of a fluorescent paclitaxel derivative binding to microtubules. *Biochemistry* 2000;39:616–23.